Chapter 2. One-Dimensional Noah's Deconvolution

Introduction

An ancient geophysicist by the name of Noah had an unusual method of reflection profiling. Noah recognized that a severe problem with his seismic exploration at sea was the multiple reflections involving the near-perfect reflector at the sea surface. That is, simply the presence of the free surface accounted for most of the disturbing multiple reflections. Being the practical man that he was, and having knowledge of the latest weather forecast, Noah proposed to collect his data in a submarine during the flood. Thus, by effectively removing the free surface reflections, the very good result was that Noah's seismograms were free of seafloor, pegleg, and structure-structure multiple reflections. Figure 2-1 illustrates Noah's recording geometry.

While we cannot record data like Noah, we may try to synthesize Noah's seismograms from ours in the computer. That is, we would like to find a transformation of the data which takes us from our geometry to Noah's. In this section we will consider a one-dimensional earth model and develop a single-channel algorithm for the transformation. In chapters 3 and 4 we will extend the analysis to waves in two dimensions.

There are good reasons to study a one-dimensional model of the earth in addition to a two-dimensional model. First of all, a large portion of the data we record is, in fact, over relatively flat, layered structure. Explorationists have long used this large component of horizontal layering to their advantage in data processing. Secondly, a one-dimensional algorithm provides a point of reference for higher dimensional algorithms. Often, numerical procedures developed

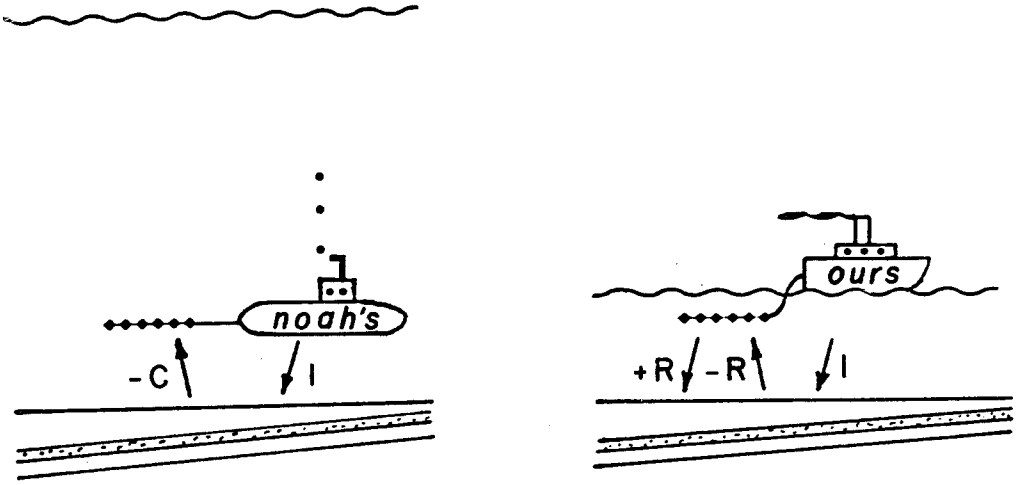

Figure 2-1. Noah's recording geometry on the left and ours on the right. Noah believed that the large problem with multiple reflections was mainly due to the presence of the free surface. By effectively removing the free surface, Noah eliminated the disturbing amount of multiple energy associated with reflections off the sea surface.

for the 1-D case may be needed in solving the 2-D problem (such as source waveform estimation). Finally, the 1-D approximation makes the problem immediately tractable and results in a very simple algorithm of practical value.

One-Dimensional Algorithm

The layered media approximation is that the earth model is a function of depth only. We will also assume that the source is a vertically incident plane wave. To synthesize Noah's seismogram from ours we place all receivers at the same datum and equate the Z-transfer function $G(Z)$ of the earth beneath the free surface as deduced from our experiment and that of Noah's. This follows from the assumption of plane layers and plane waves; that is, we may make the sweeping statement that the earth behaves as a one-dimensional, time-invariant, linear system. As such, it is completely described by the transfer function $G(Z) = U(Z) / D(Z)$ where U and D are the Z-transforms of the upcoming and downgoing waves, respectively. In the original geometry we have the upcoming waves $-R(Z)$, the surface reflection seismogram, and the downgoing waves consisting of the ideal, impulsive plane source 1 and $R(Z)$ reflecting off the free surface.

In the above definition for the reflection seismogram, being only the upcoming wave, we have excluded the possibility of recording the direct path arrival of the shot. In practice we do record a direct arrival, but because of always finite shot-receiver offset, we receive the horizontally travelling source waveform. We will later see how we may use the 1-D algorithm itself to estimate the desired vertically transmitted source waveform. Thus, we disregard as unmeasurable and unmodeled the early portion of the seismogram containing the shot waveform.

Noah's upcoming waves are defined as $-C(Z)$ while the downgoing wave is simply the shot since the free surface is absent. Thus,

$$G(Z) \triangleq \frac{U(Z)}{D(Z)}\Bigg|_{\text{surface}} \tag{2-1}$$

where U , D are the up and downgoing waves seen by the receivers. For the same earth below and same datum above we may equate the transfer functions for both geometries.

$$\frac{U(Z)}{D(Z)}\Bigg|_{\text{surface}} = \frac{-C(Z)}{1} = \frac{-R(Z)}{1+R(Z)} \tag{2-2}$$

so that the desired transformation is

$$C(Z) = \frac{R(Z)}{1+R(Z)} \tag{2-3}$$

In order to do the transformation of (2-3) a necessary condition is that $1 + R(Z)$ be causally invertible or physically realizable, since $c_t = 0$ for $t \leq 0$. In the ideal 1-D case before us, this is guaranteed since it may be shown that the quantity $1 \pm R(Z)$ is minimum-phase (Sherwood and Trorey, 1965). Thus, we may assume that any polynomial divisions by $1 + R(Z)$ will be numerically stable.

If in equation (2-3) we expand the time functions in Z and multiply we have

$$(c_0 + c_1 Z + c_2 Z^2 + \cdots)(1 + r_0 + r_1 Z + r_2 Z^2 + \cdots) = r_0 + r_1 Z + r_2 Z^2 + \cdots$$

then identifying and equating coefficients of like powers of Z such as

$$c_0 = r_0 = 0$$

$$c_1 = r_1$$

$$c_2 = r_2 - c_1 r_1$$

$$c_3 = r_3 - c_1 r_2 - c_2 r_1$$

which generalizes to the relations

$$c_t = r_t - \sum_{k=1}^{t-1} c_k r_{t-k} \qquad t = 1,2,... \qquad (2\text{-}4a)$$

or

$$r_t = c_t + \sum_{k=1}^{t-1} r_k c_{t-k} \quad , \quad \text{which define} \qquad (2\text{-}4b)$$

recursions involving the feedback of past computations. Thus, the recurrance (2-4a) indicates how to develop a new point on Noah's seismogram from the convolution of the previously computed portion onto the original reflection seismogram. Equation (2-4b) is the procedure for computing our seismogram, given Noah's. Note that, in this formulation, the reflection seismogram is composed of a primary part c_t added to a predicted, deterministic multiple part $r * c$. Therefore, equation (2-4a) may be viewed as a decomposition to yield the unpredictable information by a subtraction of the predictable multiples from the seismogram, as illustrated in Figure 2-2. Thus, like statistical prediction-error deconvolution we subtract off the self-prediction of the data. Unlike deconvolution, however, the "filter" is the deconvolved seismogram itself. Noah's deconvolution is a deterministic decomposition based on relative amplitudes. No spectral estimates or assumptions about phase need be made.

The Practical Problem

There are several problems which arise in dealing with realistic cases, either synthetic or field data. One is that of computational

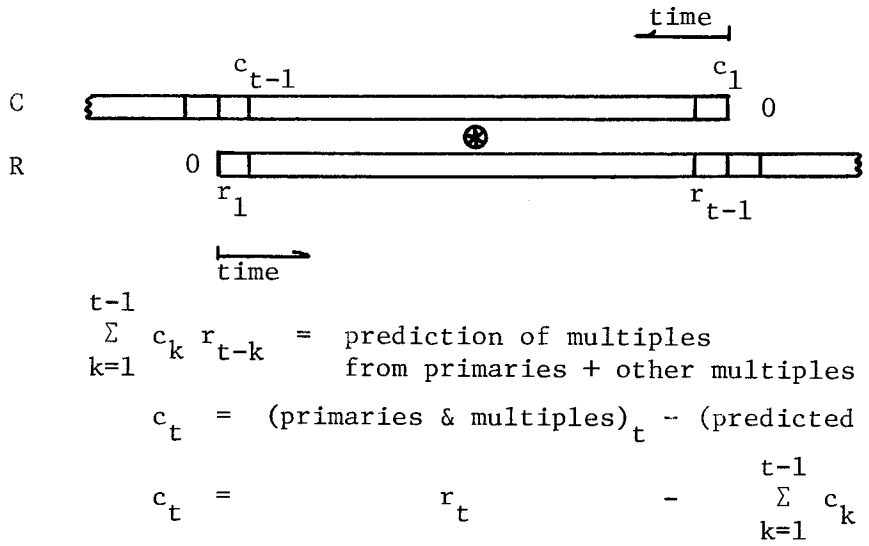

Figure 2 - 2. Noah's transformation predicts multiples by the convolution of earlier multiples onto the primaries. Noah's seismogram C operates as a prediction "filter" on the reflection data R to yield a prediction of the multiples which are then subtracted from the data. Thus, the "filter" is the deconvolved data itself.

efficiency, since the number of operations for a trace n samples long is $n(n+1)/2$ multiplies and adds. For a typical length seismogram such a growing numerical procedure quickly becomes undesirably expensive. The solution to this is recognizing and including only the important terms in the summation. This will be discussed in the following section where we consider the various classes of multiples.

The other problem of practical interest is that so far we have not taken into account a realistic source waveform of finite duration and bandwidth. We shall rewrite the transfer function equation again, this time including a vertical shot pulse $B(Z)$ originating at $t=0$. In this case our up and downgoing waves are

$$U = -\tilde{R}(Z) = -B(Z)\,R(Z) \tag{2-5a}$$

$$D = B(Z) + \tilde{R}(Z) \tag{2-5b}$$

and Noah's are

$$U = -\tilde{C}(Z) = -B(Z)\,C(Z) \tag{2-6a}$$

$$D = B(Z) \tag{2-6b}$$

where the wiggle denotes the reflected wave with B as the source instead of 1.

Thus, equating transfer functions, we have

$$\frac{\tilde{C}(Z)}{B(Z)} = \frac{\tilde{R}(Z)}{B(Z)+\tilde{R}(Z)} \tag{2-7}$$

Now, define an inverse of B to be $H(Z) \triangleq B^{-1}(Z)$, and dividing through equation (2-7) by H we have

$$\tilde{C}(Z) = \frac{\tilde{R}(Z)}{1+H(Z)\tilde{R}(Z)} \tag{2-8}$$

The result of including the source waveform affects only summation of $\tilde{c}$ onto $\tilde{r}$. Identifying and equating like powers of Z in equation (2-8) results in a similar recurrance pair similar to (2-4a) and (2-4b)

$$\tilde{c}_t = \tilde{r}_t - h * \sum_{k=1}^{t-1} \tilde{c}_k \tilde{r}_{t-k} \qquad (2\text{-}9a)$$

$$\tilde{r}_t = \tilde{c}_t + h * \sum_{k=1}^{t-1} \tilde{r}_k \tilde{c}_{t-k} \qquad (2\text{-}9b)$$

The function of the source inverse H is to modify the result of convolving $\tilde{c}$ and $\tilde{r}$. This is a modification to both scale and color since, in the process of convolving $\tilde{c}$ and $\tilde{r}$, the source waveform-squared will not only be spread out but also its center of gravity will be delayed.

Therefore, in designing the form of the inverse operator H it should not only whiten B but advance it up to its original position as illustrated in Figure 2-3. Recall, though, that we have not, in general, allowed ourselves direct access to the vertical path waveform B on the data. However, we may consider the case where the various multiples are distinctly separated in time as in figure 2-3. There we may estimate H directly from the multiples. Assuming only multiples and no primaries exist in the gate N_{3e} to N_{4e} we have that $\tilde{c}_t = 0$ for $N_{3e} < t < N_{4e}$. Further that the primary generating the multiple lies in the gate N_{1e} to N_{2e}. Thus equation (2-9a) becomes

$$0 = \tilde{r}_t - h * \sum_{k=N_{1e}}^{N_{2e}} \tilde{r}_k \tilde{r}_{t-k} \quad \text{for} \quad N_{3e} \leq t \leq N_{4e} \qquad (2\text{-}10)$$

That is, the inverse waveform may be estimated from the relation between the primary convolved on itself and the multiple. In the examples we have used a least-squares estimator for h by solving the over-

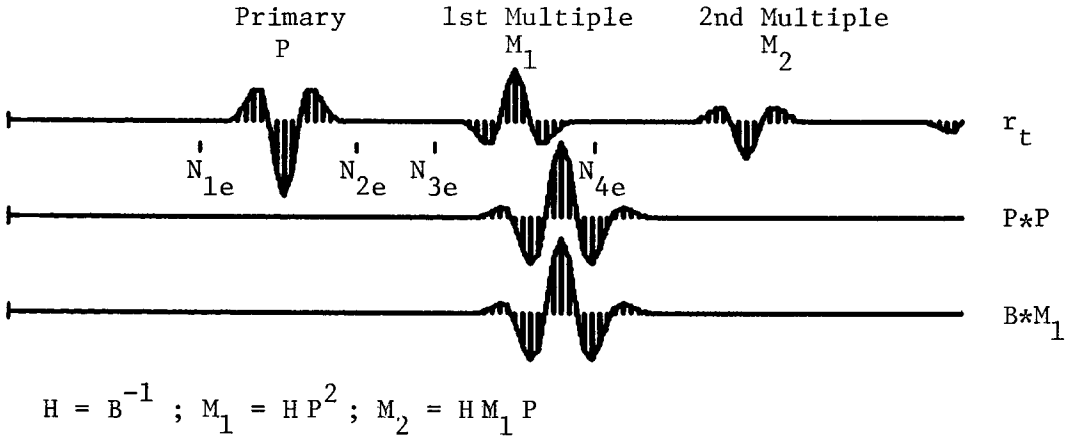

$$H = B^{-1} \; ; \; M_1 = H P^2 \; ; \; M_2 = H M_1 P$$

Figure 2 - 3. Estimation of the inverse source wavelet H(Z).

H is designed to be anticausal such that the source waveform-squared is contracted and pushed back in time. Where the multiples are distinct in time we may estimate h from the relationship between the primary convolved with itself and the 1st multiple, $M_1 = h * P * P$.

determined problem

$$\min_{h} \sum_{t=N_{3e}}^{N_{4e}} \left[\tilde{r}_t - h * \sum_{k=N_{1e}}^{N_{2e}} \tilde{r}_k \, \tilde{r}_{t-k} \right]^2 \qquad (2\text{-}11)$$

where h is chosen to be anticausal.

Therefore, having estimated h, we apply it to all the data $\tilde{r}$ and compute Noah's seismogram with the recurrance

$$\tilde{c}_t = \tilde{r}_t - \sum_{k=1}^{t-1} \tilde{c}_k \, r_{t-k} \quad , \quad r_{t-k} = h * \tilde{r}_{t-k} \qquad (2\text{-}12a)$$

or synthesize reflection data by

$$\tilde{r}_t = \tilde{c}_t + \sum_{k=1}^{t-1} \tilde{r}_k \, c_{t-k} \quad , \quad c_{t-k} = h * \tilde{c}_{t-k} \qquad (2\text{-}12b)$$

Classes of Multiples

The other problem of practical interest was noted earlier as involving the computational efficiency in dealing with typical length records. By careful gating of the summation in the recursion, the computations may largely be reduced to a linear function of record length. Additionally, we gain a certain amount of control over the various classes of multiple reflections we need synthesize or remove. Running the recursion without any gates, as in equations (2-12a,b), will accomodate all classes of multiples involving the free surface reflection. That is, in computing Noah's seismograms from ours, we correctly model and eliminate all classes of multiples that were absent in Noah's geometry. The only multiples that are left unmodeled are those involving intrabed reflections. We may define intrabed multiples as those rays which suffer a reflection on their upcoming path with the exception of reflections at

the free surface. Thus, since the Noah transformation does not model intrabed energy it remains in the inverted or deconvolved data. As will be discussed in chapter 3, in a practical application intrabed multiples comprise a relatively small portion of the multiple energy distribution. The important thing is that the disturbing amount of free surface multiple energy is properly treated within the framework of the simple model.

By neglecting intrabed multiples in the calculation, Noah's seismogram $\tilde{c}$ consists of only primary reflections or, to use the term loosely, reflection coefficients. The summation in (2-12,a,b) may be regarded as the convolution of r (downgoing ray)with $\tilde{c}$ (reflectors) to yield a prediction of the multiple reflection. In Figure 2-4 the ray path of the various classes of multiples are illustrated. Seafloor multiples (a) and one of the structure pegleg paths (c) are generated by the interaction of the downgoing ray and the seafloor reflector (say bounded by the gate $N_{1s} - N_{2s}$). The other ray path for structure peglegs (b) is due to the reverberatory front portion of the downgoing ray (say, with a time gate of $N_{1\ell} - N_{2\ell}$) interacting with the structure reflector. Structure-structure paths (d) are generated directly in the center of the summation. Therefore, time-coincident multiple paths may be distinguished by splitting the summation in equations (2-12) into gates where each class is generated. Since the gates of paths (b) and (d) depend on travel time, such a description by gates is valid for any number of reflectors.

Therefore, the computations can be made quite economical with just the knowledge that the seafloor lies within some approximate time gate. It is important, from a practical point of view, that the precise depth

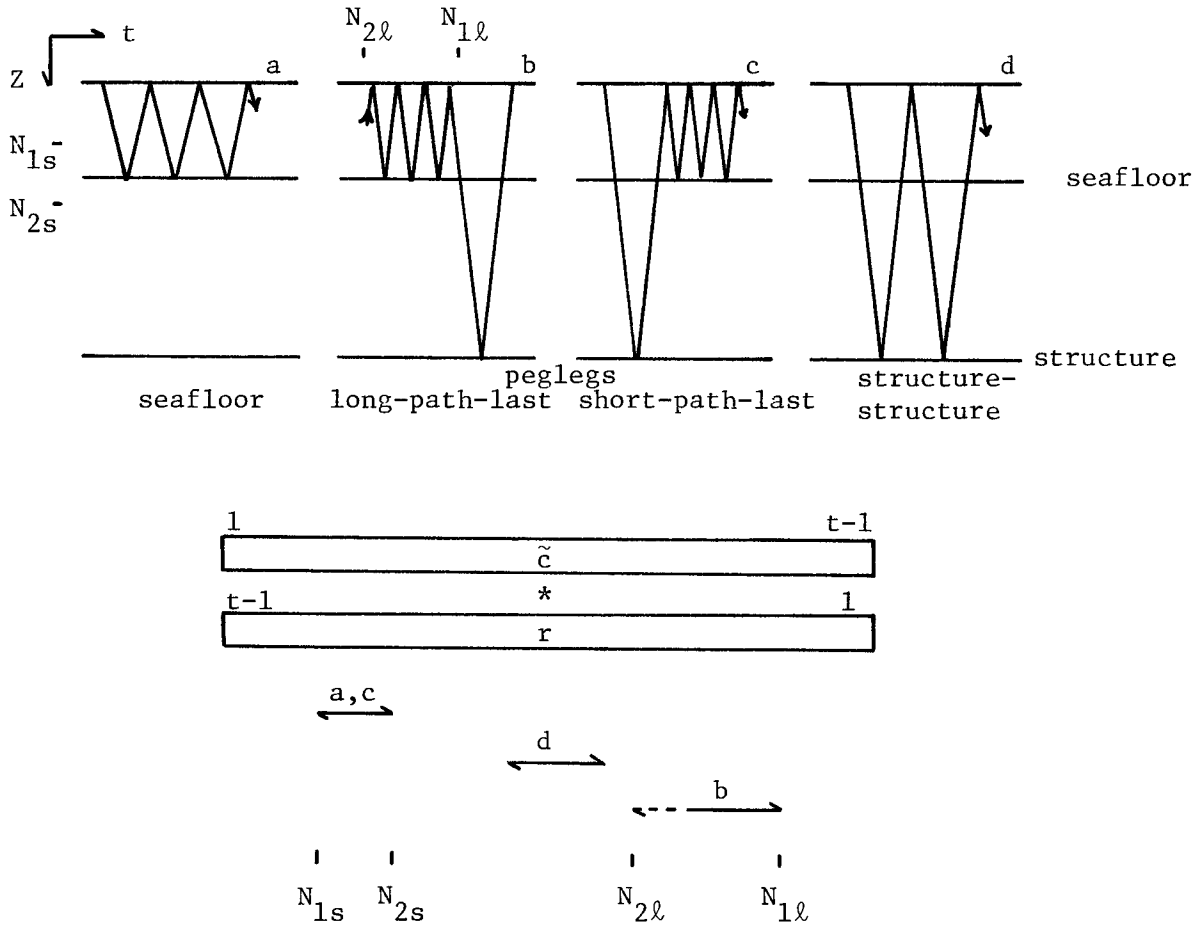

Figure 2 - 4. Gating arrangement for the convolution of the downgoing ray r with the reflectors $\tilde{c}$. By recognizing where the various multiples arise in the summation, we may eliminate a large amount of unnecessary calculations. For a seafloor reflector in the time gate N_{1s} to N_{2s} the seafloor multiples (a) and short-path-last peglegs (c) are modeled in the corresponding gate on $\tilde{c}$. Long-path-last peglegs (b) result from simple seafloor multiples leaving the water layer and reflecting off the structure. Gating-in that early portion of r (downgoing ray) including the seafloor reverberations models these arrivals. In practice we limit consideration to two or three bounces as the $N_{1\ell}$ to $N_{2\ell}$ gate. The structure-structure multiples arise from terms directly in the centers (k=t/2) of the summation.

to the seafloor is not required. In the examples, we have neglected the structure-structure term explicitly, although it is usually included in one of the two gates, in using

$$\tilde{c}_t = \tilde{r}_t - \sum_{k=N_{1s}}^{\max(t-N_{1\ell},\, N_{2s})} \tilde{c}_k\, r_{t-k}\,, \quad \text{for} \quad N_{1s} \leq (t-N_{2\ell}) \leq N_{2s} \qquad (2\text{-}13)$$

and

$$\tilde{c}_t = \tilde{r}_t - \sum_{k=N_{1s}}^{N_{2s}} \tilde{c}_k\, r_{t-k} - \sum_{k=N_{1\ell}}^{N_{2\ell}} r_k\, \tilde{c}_{t-k}\,, \quad \text{for} \quad t > N_{2s} + N_{2\ell} \qquad (2\text{-}14)$$

Synthetic and Field Examples

Figure 2-5 illustrates the use of the one-dimensional algorithm in modeling seafloor and pegleg multiple reflections. The frame at the left of the figure is Noah's seismogram $\tilde{C}$ recorded over an undulating seafloor and a deep faulted structure. Ignoring long-delay intrabed reflections this is the reflector model. The center frame is the 1D reflection seismograms $\tilde{R}$ as calculated with equation (2-12b). With successive reflections in the water layers the seafloor multiples become increasingly stretched by the seafloor topography. Beneath the primary reflector at .7 sec. the structure pegleg arrivals appear. They assume the geometry of the primary structure stretched by the seafloor. Due to the multiplicity of paths, pegleg multiples decay at a slower rate than simple seafloor multiples.

Using the center frame as data, the inverse source waveform h was estimated from the relationship between the seafloor primary and the first seafloor multiple. The inverse wavelet was estimated from

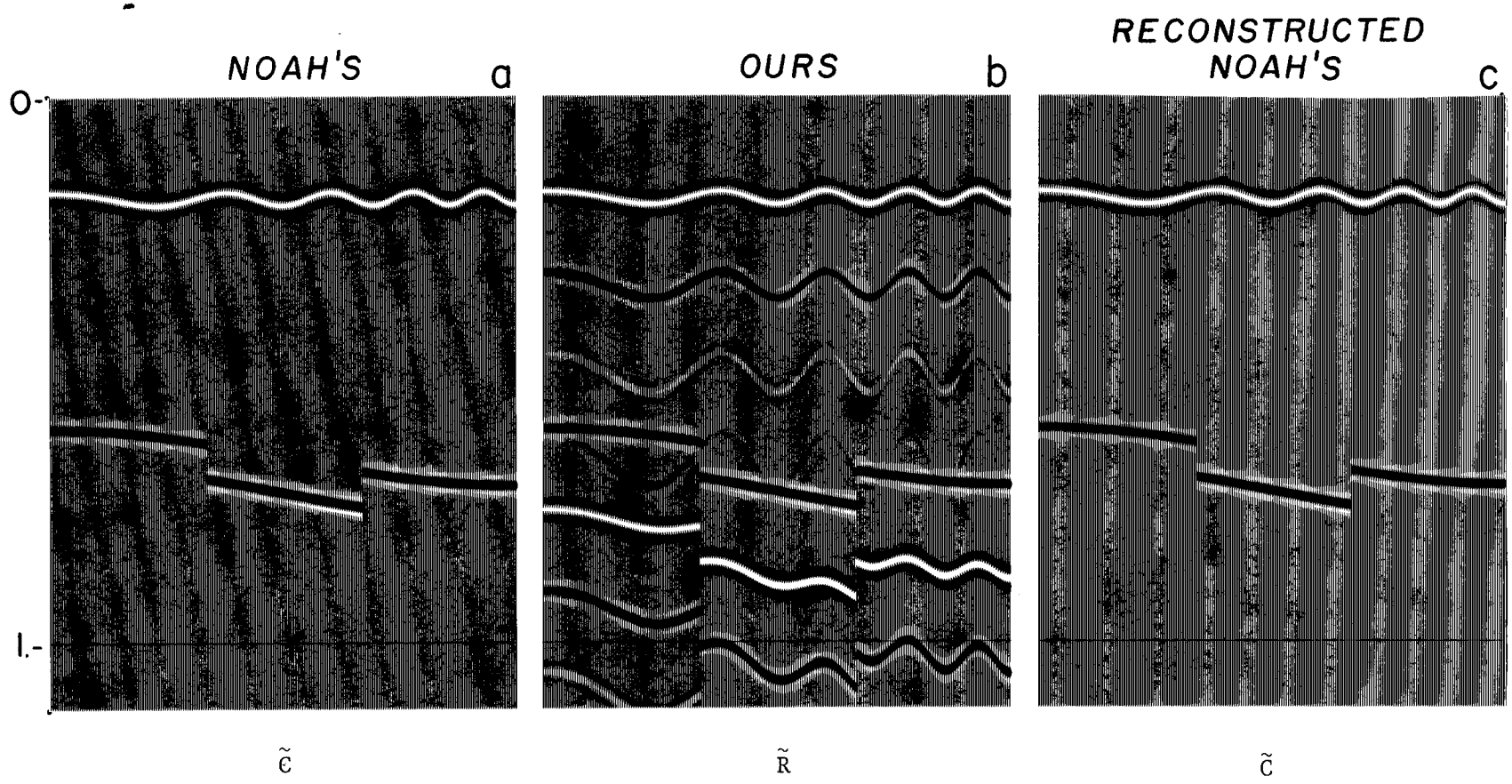

Figure 2 - 5. The reflection coefficient model or Noah's seismograms are given at the frame to the left. Using the forward transformation the 1-D reflection seismogram is computed in the center frame. For display purposes a uniform exponential gain of 24 db/sec. has been applied to all three frames. Using the center frame as data, an estimate of the source waveform h was derived from the relationship between the self-convolution of the seafloor and the first seafloor multiple. Applying this estimate to all the traces, the inverse transformation was computed. The frame at the right is the reconstruction of Noah's seismogram from the reflection seismogram.

a single channel and applied to all the data. The inverse transformation of equation (2-12a) was then used to compute Noah's seismogram from ours. The frame at the right is the reconstruction of Noah's seismogram.

Figure 2-6 illustrates the inverse transformation applied to a section of field data. The center frame is a true amplitude near-trace section recorded off the eastern shelf of Canada. The seafloor reflection coefficient is relatively large (≈ 0.2) in this area giving rise to a very strong pattern of seafloor multiples and peglegs. In many instances the multiple arrivals overlie and mask the primary reflections as in the case of the flat lying structure at 1.8 sec.

As in the synthetic example, an estimate of the inverse source wavelet h was derived from the seafloor primary and first seafloor multiple by equation (2-11). This single estimate was then applied to each trace prior to doing the inverse transformation. The frame at the right is the near-trace section after Noah's deconvolution. Note that the fourth seafloor multiple M_4 interfering with the primary arrival has been predicted and subtracted. Also note that the structure peglegs Pm below 2.0 sec. have been almost completely extinguished. The only noticeable problem appears to be with the first seafloor multiple. This may be due to some residual normal moveout or problems in the process of true amplitude recovery. The important thing is that the correct amplitudes have been predicted for the pegleg multiple reflections and that we may conclude, as did Noah, that free surface multiples account for most of the disturbing amount of multiple energy.

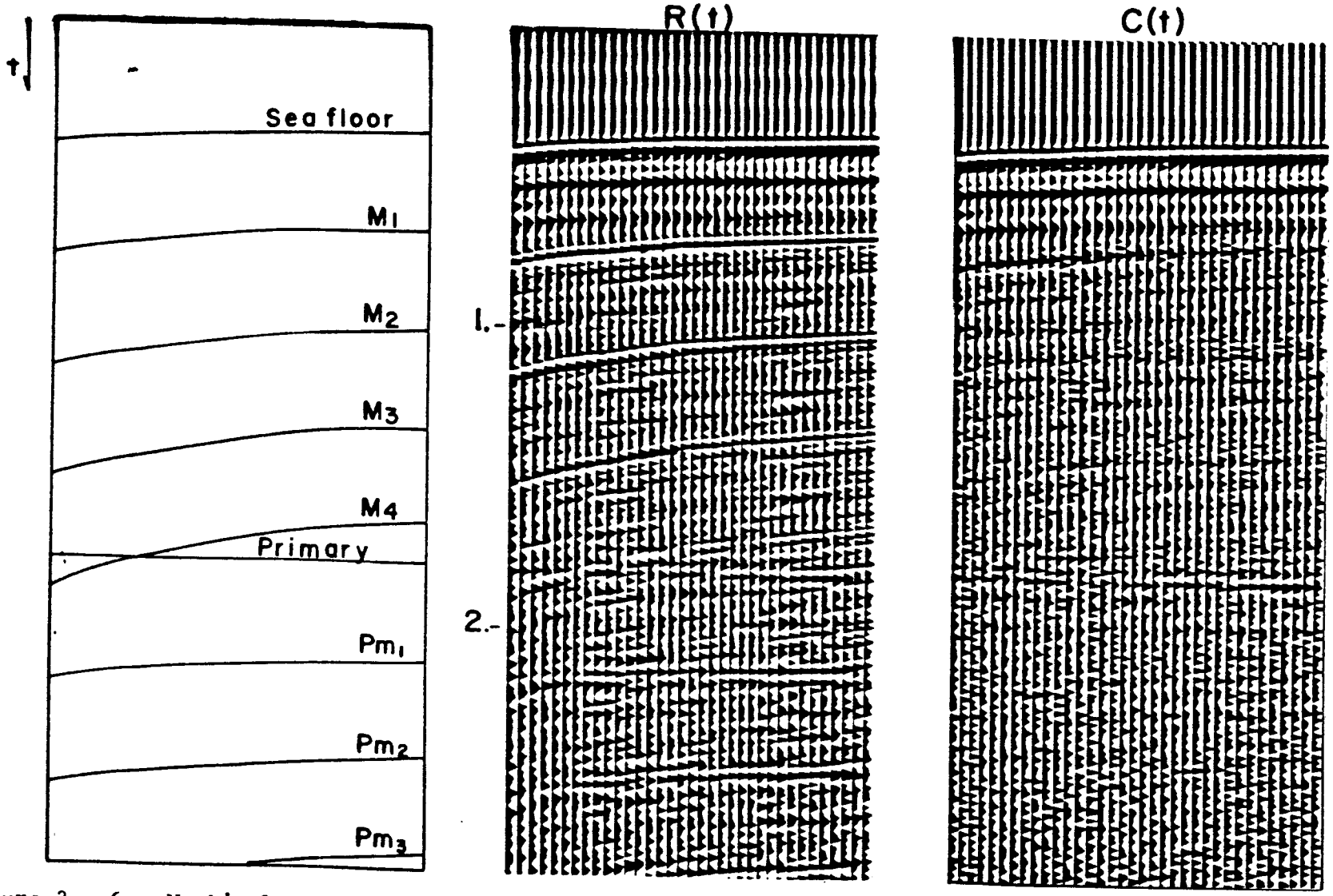

Figure 2 - 6. Noah's 1-D deconvolution of field data. The center frame is a near-trace section of reflection data recorded off eastern Canada. The frame at the left depicts the seafloor reflection and the very strong seafloor multiples $M_1,...M_4$. At about 1.8 sec. there is a nearly flat lying primary reflector partially masked by M_4. Below this are the structure peglegs Pm_1, Pm_2. Pm_3 . The frame to the right is the section processed with equations (2-12a). Note that the disturbing amount of multiple reflections have been correctly predicted and removed. No frequency filtering was necessary since the transformation does not alter the original color of the data.